Neuron 52, 679–690, November 22, 2006 ©2006 Elsevier Inc. DOI 10.1016/j.neuron.2006.09.035

Hyperekplexia Phenotype of Glycine Receptor α1 Subunit Mutant Mice Identifies Zn^{2+} as an Essential Endogenous Modulator of Glycinergic Neurotransmission

Klaus Hirzel,[1,4,5] Ulrike Müller,[1,4,6] A. Tobias Latal,[2,4] Swen Hülsmann,[2] Joanna Grudzinska,[1,7] Mathias W. Seeliger,[3] Heinrich Betz,[1,*] and Bodo Laube[1,8]

[1] Abteilung Neurochemie
Max-Planck-Institut für Hirnforschung
Deutschordenstrasse 46
60528 Frankfurt am Main
Germany

[2] Zentrum Physiologie und Pathophysiologie
Abteilung Neuro/Sinnesphysiologie und
DFG-Forschungszentrum für Molekular-Physiologie des Gehirns
Humboldtallee 23
37073 Göttingen
Germany

[3] Retinal Electrodiagnostics Research Group
Department of Pathophysiology of Vision and Neuroophthalmology
Schleichstrasse 4
Universityof Tübingen
72076 Tübingen
Germany

Summary

Zn^{2+} is thought to modulate neurotransmission by affecting currents mediated by ligand-gated ion channels and transmitter reuptake by Na^+-dependent transporter systems. Here, we examined the in vivo relevance of Zn^{2+} neuromodulation by producing knockin mice carrying the mutation D80A in the glycine receptor (GlyR) α1 subunit gene (*Glra1*). This substitution selectively eliminates the potentiating effect of Zn^{2+} on GlyR currents. Mice homozygous for *Glra1*(D80A) develop a severe neuromotor phenotype postnatally that resembles forms of human hyperekplexia (startle disease) caused by mutations in GlyR genes. In spinal neurons and brainstem slices from *Glra1*(D80A) mice, GlyR expression, synaptic localization, and basal glycinergic transmission were normal; however, potentiation of spontaneous glycinergic currents by Zn^{2+} was significantly impaired. Thus, the hyperekplexia phenotype of *Glra1*(D80A) mice is due to the loss of Zn^{2+} potentiation of α1 subunit containing GlyRs, indicating that synaptic Zn^{2+} is essential for proper in vivo functioning of glycinergic neurotransmission.

*Correspondence: neurochemie@mpih-frankfurt.mpg.de
[4] These authors contributed equally to this work.
[5] Present address: Roche Diagnostics GmbH, Centralized Diagnostics R & D Nonnenwald 2, 82377 Penzberg, Germany.
[6] Present address: Institute for Pharmacy and Molecular Biotechnology, University of Heidelberg, Im Neuenheimer Feld 364, 69120 Heidelberg, Germany.
[7] Present address: Biochemistry Department, Conway Institute for Biomolecular and Biomedical Research, University College Dublin, Belfield, Dublin 4, Ireland.
[8] Present address: AG Zelluläre Neurophysiologie, FB Biologie, Technical University of Darmstadt, Schnittspahnstrasse 3, 64287 Darmstadt, Germany.

Introduction

The mammalian central nervous system (CNS) contains high concentrations of the divalent metal ion Zn^{2+}. Although acute Zn^{2+} deficiency impairs brain development and function in experimental animals and humans (overview in Choi and Koh [1998]), the roles of Zn^{2+} in the CNS remain enigmatic. Ninety percent of the total Zn^{2+} in brain tissue is tightly bound to proteins, and only 10% exists in a pool of chelatable "free" Zn^{2+}. This chelatable Zn^{2+} is not evenly distributed in the brain but highly enriched in distinct glutamatergic nerve terve terminals (Choi and Koh, 1998). Furthermore, enrichment of Zn^{2+} at selected inhibitory synapses in cerebellum and spinal cord has also been reported (Velázquez et al., 1999; Jo et al., 2000; Danscher et al., 2001; Wang et al., 2001, 2002; Danscher and Stoltenberg, 2005). Estimates of free Zn^{2+} concentrations in the CNS vary between 100 and 200 nM in the cerebrospinal fluid and >200 μM within specific synaptic regions (Choi and Koh, 1998). Elevated concentrations of Zn^{2+} (>100 μM) may contribute to neuronal cell death during brain ischemia, seizures, trauma, and neurodegeneration (Choi and Koh, 1998; Doraiswamy and Finefrock, 2004), whereas lower levels of Zn^{2+} (<10 μM) protect neurons against glutamate-induced cell death (Chen and Liao, 2003; Chandra et al., 2005). Hence, proper regulation of Zn^{2+} homeostasis is thought to be crucial for brain function and development.

At synapses, Zn^{2+} is highly enriched in synaptic vesicles, from which it can be coreleased with glutamate in an activity-dependent manner (Assaf and Chung, 1984). Microfluorescence imaging of Zn^{2+} secretion during presynaptic stimulation has provided evidence for a quantal mode of Zn^{2+} release from hippocampal Mossy fiber terminals (Li et al., 2001; Qian and Noebels, 2005); however, the interpretation of the signals obtained in these studies has been a matter of debate (see Kay [2006]). The loading of synaptic vesicles with releasable Zn^{2+} is thought to be mediated by ZnT3, a member of the SLC30 superfamily of Zn^{2+} transporters (Cole et al., 1999). In addition, synaptic Zn^{2+} concentrations are controlled by other Zn^{2+} transporters of the ZnT (SLC30) and Zip (SLC39) families as well as by Zn^{2+}-sequestering proteins, like metallothioneins (Baranano et al., 2001; Kambe et al., 2004; Smart et al., 2004). Since Zn^{2+} modulates both current responses mediated by excitatory and inhibitory neurotransmitter receptors and the efficacy of transporter driven neurotransmitter reuptake (Smart et al., 2004), synaptically released Zn^{2+} has been proposed to function as an important regulator of synaptic transmission and plasticity (Lu et al., 2000; Vogt et al., 2000) and/or "atypical neurotransmitter" (Baranano et al., 2001). This concept has, however, been challenged because (1) mice deficient in ZnT3 were found to be behaviorally normal despite a loss of synaptic Zn^{2+} staining (Cole et al., 1999) and (2) the available Zn^{2+} imaging techniques have been argued to be particularly sensitive to artifacts (Kay, 2006).

In this study, we have chosen a genetic approach to unravel the importance of Zn^{2+} for synaptic

transmission. Previously, we and others have shown that Zn^{2+} affects the function of the strychnine-sensitive glycine receptor (GlyR; Bloomenthal et al., 1994; Laube et al., 1995), which mediates postsynaptic inhibition in motor and sensory pathways (overview in Betz and Laube [2006]). In spinal neurons and cells expressing recombinant GlyRs, low micromolar (<10 μM) concentrations of Zn^{2+} enhance glycinergic currents, whereas higher concentrations (>10 μM) have an inhibitory effect. The effects of low concentrations of Zn^{2+} have been attributed to an increase in agonist affinity resulting from decreased agonist dissociation; higher Zn^{2+} concentrations produce a voltage-independent block by reducing the efficacy of channel opening (Laube et al., 2000; Lynch, 2004). Also, GlyR-mediated miniature inhibitory postsynaptic currents (mIPSCs) have been shown to be modulated by Zn^{2+} (Suwa et al., 2001; Laube, 2002), indicating that Zn^{2+} regulation is effective at synaptic sites. Mutational studies have localized the Zn^{2+} binding sites mediating potentiation and inhibition of GlyRs in distinct regions of the N-terminal extracellular domain of GlyR α subunits (Laube et al., 2002; Lynch, 2004). Specifically, residues D80, E192, D194, and H107, H109, T112 of the adult-type GlyR α1 subunit have been found to constitute important determinants of Zn^{2+} potentiation and inhibition, respectively (Lynch et al., 1998; Harvey et al., 1999; Laube et al., 2000; Miller et al., 2005). Neutralization of the γ-carboxylate of aspartate 80 by glycine or alanine substitution selectively eliminates Zn^{2+} potentiation without affecting channel conductance and receptor kinetics (Lynch et al., 1998; Laube et al., 2000). Here, we introduced the D80A substitution into the murine GlyR α1 gene locus (*Glra1*) via homologous recombination. Knockin mice homozygous for *Glra1*(D80A) show a phenotype, which mimicks that of human hyperekplexia (hereditary startle disease) patients and *spasmodic* or *spastic* GlyR mutant mice and is indicative of decreased glycinergic inhibition (Schofield, 2002). Our results indicate that potentiation of the GlyR by synaptic Zn^{2+} is essential for proper glycinergic inhibition in vivo.

Results

Generation of *Glra1*(D80A) Mice and GlyR Protein Expression

The targeting strategy used for introducing the D80A substitution into exon 4 of *Glra1* is depicted in Figure 1A. Using a replacement type targeting vector, the mutation was introduced into ES cells by homologous recombination together with a diagnostic XbaI restriction site and a floxed neomycin resistance cassette (neo), positioned in the 3′ adjacent intron. Homologous recombination events were identified by PCR, and confirmed by Southern blot analysis (Figures 1A and 1B). In a second step, the neo selection marker was deleted by transient transfection with a Cre recombinase expression vector (Figure 1C). The resulting mutant ES cells were injected into blastocysts and gave rise to two germline-transmitting chimeras. These animals sired heterozygous offspring without obvious abnormalities in morphology and behavior. Intercrosses of heterozygous animals generated *Glra1*(D80A) homozygous, heterozygous, and WT animals at the expected Mendelian ratios. Correct introduction of the mutation *Glra1*(D80A) was confirmed by Southern blotting (Figure 1D) of XbaI-digested DNA and corroborated by sequencing the exon 4 region of the mutant locus (data not shown).

To examine whether GlyR α1 subunit expression is unaltered in homozygous *Glra1*(D80A) mice, we analyzed GlyR expression in spinal cord tissue from postnatal day 21 (P21) mice. Immunoblot analysis of spinal membrane preparations with an antibody which recognizes all GlyR α subunits (mAb4a) or an antibody specific for the α1 subunit (mAb2b) showed similar expression levels in all genotypes examined (Figures 2A and 2B). Neither total GlyR α nor α1 levels were significantly altered by the D80A substitution as revealed by normalizing densitometrically determined band intensities to syntaxin expression (mAb4a immunoreactivity in homozygous *Glra1*(D80A)—115% ± 10% of WT; n = 6; p > 0.05; mAb2b immunoreactivity in homozygous *Glra1*(D80A)—127% ± 34% of WT; n = 5; p > 0.05). Since the GlyR α1 subunit is the predominant subunit in adult spinal cord and accounts for high-affinity [^{3}H]strychnine binding, we also performed binding assays on spinal cord membrane preparations at ligand concentrations ranging from 1 to 200 nM. [^{3}H]strychnine bound to WT and homozygous *Glra1*(D80A) membranes with similar dissociation constants (K_Ds of 13.2 ± 3.2 nM and 24.8 ± 5.9 nM; n = 3; p > 0.05) and B_{max} values (874 ± 76 and 1112 ± 165 fmol/mg protein, n = 3; p > 0.05; Figure 2C). Thus, the D80A mutation does not significantly affect receptor expression or ligand binding properties in vivo. We also examined the synaptic localization of the α1(D80A) subunit by performing immunocytochemistry on spinal cord sections with the α1-specific antibody mAb2b (Figure 2D). The punctate distribution of mAb2b staining, indicative of postsynaptically clustered GlyRs, was indistinguishable between WT and homozygous *Glra1*(D80A) sections, as revealed by respective cluster counts (43 ± 17 and 51 ± 13 puncta per 100 μm^2, respectively; n = 4 each; p > 0.05; Figure 2E). We therefore conclude that the D80A mutation has no significant effects on GlyR expression and synaptic localization.

Homozygous *Glra1*(D80A) Mice Develop a Severe Neuromotor Phenotype

During the second postnatal week, at around P12, homozygous *Glra1*(D80A) mice developed a severe neuromotor phenotype characterized by an increased muscular tone and inducible tremor, which persisted throughout adulthood. Nevertheless, the homozygous animals were fertile, survived normally, and showed only a marginal reduction in body weight (<10%) as compared to their WT and heterozygous littermates (data not shown). To characterize the phenotypic properties of adult homozygous *Glra1*(D80A) mutant mice more closely, simple handling assays were performed. When picked up by the tail, homozygous mutants displayed a characteristic hind feet clasping behavior (Figure 3A). In contrast, WT and heterozygous mice balanced their position by spreading out the legs (Figure 3A). As a second criterion to evaluate neuromotor performance, littermates were screened for the development of tremor after suspending them by their tails onto an electromechanical transducer, as described previously

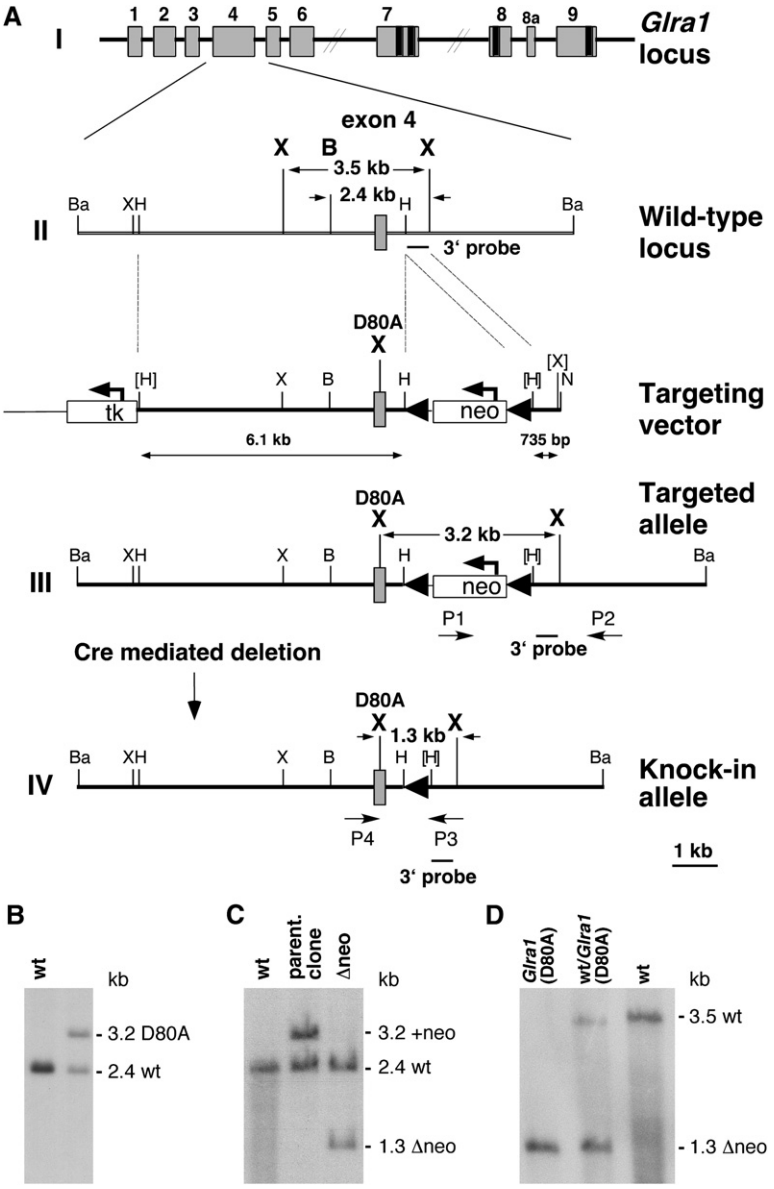

Figure 1. Generation of *Glra1*(D80A) Mice

(A) Gene targeting strategy. I: Schematic representation of the *Glra1* locus. Exons are indicated by gray boxes and transmembrane domains by black boxes within exons. II: The D80A substitution was introduced into ES cells by using a replacement type targeting vector which carried the mutation together with an adjacent silent diagnostic XbaI restriction site and a floxed (triangles) intronic neomycin selection cassette. III: Targeted locus after homologous recombination. The neomycin cassette was removed by transfecting ES cells carrying the mutant locus with a Cre expression vector. IV: Resulting ES cell clones were used for blastocyst injection. Arrows indicate primers used for PCR screening. The 3′-probe flanking the targeting vector is drawn as a solid bar. B: BclI; H: HindIII; N: NotI; X: XbaI; Ba: BamHI.

(B) Homologous recombination in ES cell clones. Insertion of the construct is revealed by Southern blot analysis using a BclI/XbaI digest of genomic DNA. The 3′ probe hybridizes to a 2.4 kb WT and a 3.2 kb mutant fragment.

(C) Cre-mediated deletion of the neomycin resistance cassette in ES cell clones is confirmed by Southern blot analysis of genomic DNA using a BclI-XbaI digest: the 3′ probe hybridizes to a 2.4 kb WT and a 1.3 kb mutant fragment, in contrast to the 3.2 kb mutant fragment seen in the parental ES cells.

(D) Southern blot analysis of genomic DNA using a XbaI digest shows that the 3′ probe hybridizes to a 3.5 kb WT, or a 1.3 kb mutant fragment, or both, in WT and homozygous or heterozygous mutant animals, respectively.

(Becker et al., 2002). In contrast to WT littermates, homozygous *Glra1*(D80A) mice developed inducible tremor, as demonstrated by high amplitudes of the electromechanical tracings which reflect tremor-induced movements (Figure 3B). Also, the righting response of the mutants was strongly impaired. WT animals immediately turned themselves over to get back on their feet (Figure 3C). In contrast, homozygous *Glra1*(D80A) mice displayed a mean righting time of >10 s (Figure 3C). Furthermore, footprint analysis disclosed clear differences in motor performance. WT animals displayed alternating positioning of hind- and forepaws, resulting in overlapping footprints and a uniform gait width (Figure 3D). In contrast, homozygous *Glra1*(D80A) mice produced traces that never showed overlapping footprints (Figure 3D). Quantification of the gait analysis revealed that homozygous *Glra1*(D80A) show a significantly shorter stride (WT, 61 ± 11 mm versus *Glra1*(D80A), 38 ± 9 mm; n = 7; $p < 0.05$), as well as a narrower base of the hind limbs (WT, 35 ± 7 mm versus *Glra1*(D80A), 27 ± 6 mm; n = 7; $p < 0.05$).

Altered Sensory Processing in Homozygous *Glra1*(D80A) Mice

To address whether adult homozygous *Glra1*(D80A) mice also show alterations in sensory functions, we analyzed parameters of visual and acoustic signal processing. First, we recorded dark- (DA) and light-adapted (LA) electroretinograms (ERGs) from homozygous *Glra1* (D80A) and WT mice (n = 6, each). Figure 4A shows representative DA and LA ERGs recorded from a WT and a homozygous *Glra1*(D80A) mouse in response to full-field flash stimuli at ten different stimulus intensities. We found a moderate increase in scotopic (DA) b-wave amplitude in homozygous *Glra1*(D80A) mice, which was even more prominent under LA conditions when cones are stimulated (Figures 4A and 4B, indicated by filled arrows). However, no difference was seen in the

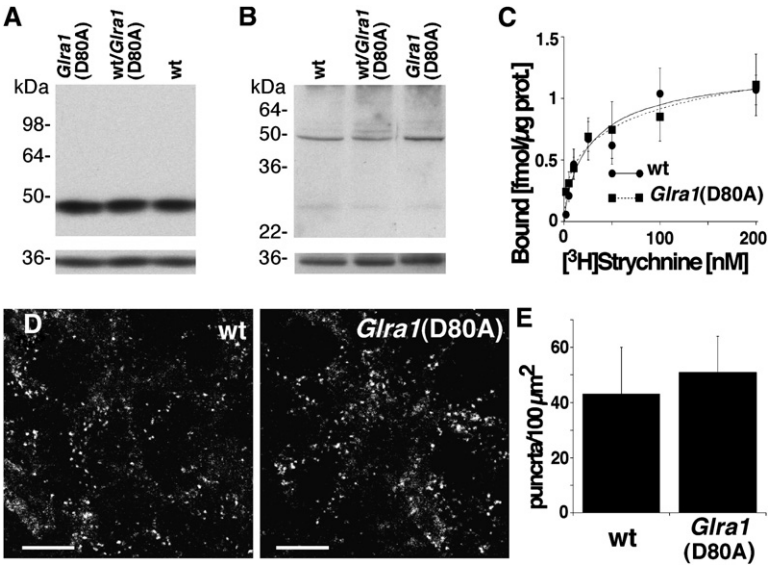

Figure 2. GlyR Expression in *Glra1*(D80A) Mice

(A–D) Expression of WT and *Glra1*(D80A) subunits in spinal cord.

(A and B) Western blot analysis of spinal cord fractions prepared from P21 WT, heterozygous, and homozygous *Glra1*(D80A) littermates, using antibodies recognizing (A) all GlyR α subunits (mAb4a) or (B) only the GlyR α1 subunit (mAb2b). Equal amounts of protein were loaded and probed with the indicated antisera. Bottom lanes: parallel detection of syntaxin was used as internal loading control. Note that expression levels are similar between genotypes.

(C) [^{3}H]Strychnine binding to spinal cord membranes from WT (solid line) and homozygous *Glra1*(D80A) (dotted line) mice.

(D) Transversal sections through the lumbar spinal cord of P21 WT and homozygous *Glra1* (D80A) littermates were processed for immunohistochemistry with mAb2b. Note similar punctate GlyR α1 staining. Scale bars, 5 μM.

(E) Quantification of α1 GlyR subunit puncta in spinal cord sections of WT and homozygous *Glra1*(D80A) littermates (n = 4, each).

Error bars indicate ± SEM.

case of the a-wave (Figures 4A and 4B, indicated by open arrows). Plotting the intensity response functions for the b-wave peak amplitudes revealed significant differences (Figure 4C; n = 6). Whereas in the DA condition the median of the b-wave amplitude in homozygous *Glra1*(D80A) mice was only slightly above the 95% quantile of that of the WT controls (the upper limit of the normal range), the median of the b-wave amplitude in the LA condition was significantly increased in homozygous *Glra1*(D80A) mice (Figure 4C). Furthermore, the mice carrying the D80A substitution had increased photopic oscillatory potentials (OPs), seen as rhythmic oscillations superimposed on the b-wave of the ERG (compare OPs of WT and homozygous *Glra1*(D80A) mice in Figures 4A and 4B). Thus the *Glra1*(D80A) substitution alters transmission of the visual signal by bipolar cells (b-wave) and AII amacrine cells (OPs), consistent with an impaired glycinergic suppression of cone signal transmission in *Glra1*(D80A) mice.

An increased acoustic startle response (ASR) is a hallmark of mutations affecting GlyR genes and seen in both mice and humans (Schofield, 2002). We also found an enhanced response of homozygous *Glra1*(D80A) mice to sudden loud acoustic stimuli (ASR), as detected by

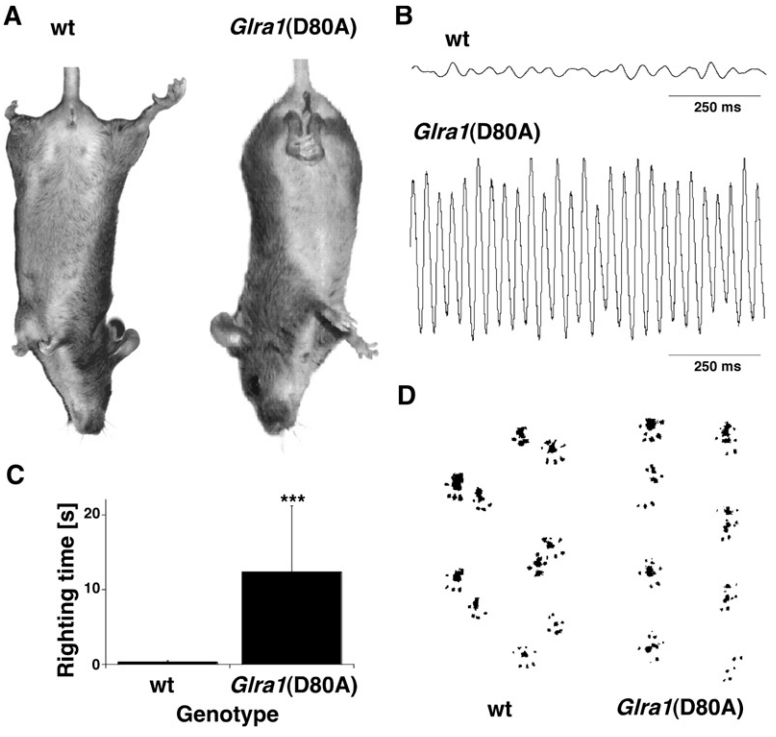

Figure 3. Motor Behavior of Homozygous *Glra1*(D80A) Mice

(A) Hind feet clasping phenotype in adult *Glra1*(D80A) mice.

(B) Electromechanical tracings of induced tremor-derived movement recorded from WT and *Glra1*(D80A) homozygous animals positioned as in (A). The amplitudes are proportional to the strength of movement recorded over time. Note the appearance of strong tremor in *Glra1*(D80A) mice.

(C) Righting time. The time required to right after being turned to the back was significantly prolonged in *Glra1*(D80A) mutants as compared to WT animals (n = 8; $p < 0.01$).

(D) Representative footprints of WT and *Glra1*(D80A) animals. Notice the "spastic" gait characterized by a decreased stride width of the hindlimbs and nonoverlapping forelimb and hindlimb strides.

Error bars indicate ± SEM.

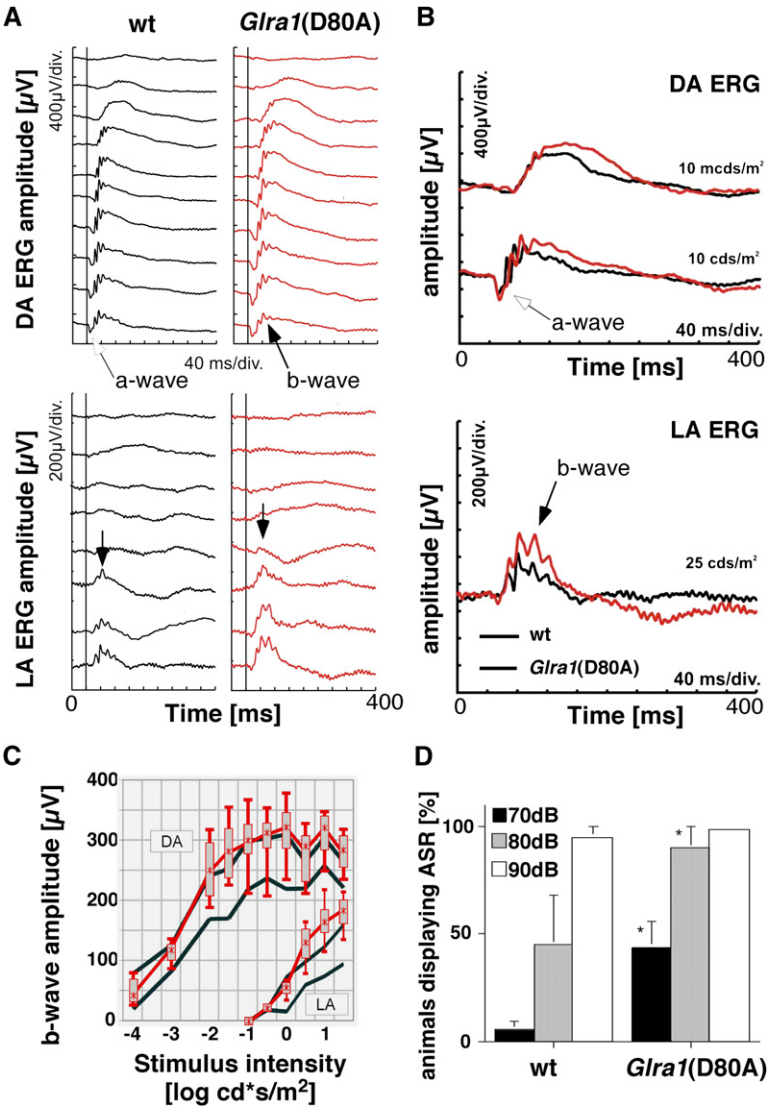

Figure 4. Sensory Perception in Homozygous *Glra1*(D80A) Mice

(A–C) Electrophysiological evaluation of retinal function in 3-month-old homozygous *Glra1*(D80A) mice.

(A) Individual traces of dark- and light-adapted ERGs recorded from WT (black) and homozygous *Glra1*(D80A) (red) mice in response to stimuli of increasing intensities. Note differences between WT and *Glra1*(D80A) mice in photopic b-wave amplitude at higher flash intensities (b-wave and a-wave are indicated by filled and open arrows, respectively).

(B) Superposition of responses shown in (A). By increasing stimulus luminance, the difference in b-wave but not a-wave amplitudes becomes obvious (indicated by solid arrow).

(C) Qualitative comparison of homozygous *Glra1*(D80A) and WT mice. b-Wave amplitudes plotted as a function of the logarithm of flash intensity. Data are from six homozygous *Glra1*(D80A) and WT littermates each. Crosses indicate the median, boxes the 25%–75% quantile range and bars the 5% and 95% quantiles, respectively, of the *Glra1*(D80A) data (red). The *Glra1*(D80A) mice show significantly larger responses in the cone-driven light-adapted ERG than WT controls (5% and 95% quantiles of WT are indicated in black). DA: dark-adapted; LA: light-adapted.

(D) ASR incidence in WT and homozygous *Glra1*(D80A) mice at three different stimulus intensities (70–90 dB). Note significantly increased ASRs to 70 and 80 dB stimuli in homozygous *Glra1*(D80A) as compared to WT mice ($n = 7$; $p < 0.05$).

Error bars indicate ± SEM.

coordinated muscle contraction. When measuring ASRs to three different stimulus intensities, mutant mice showed already at relatively low intensity levels (70 dB) a pronounced startle reaction, whereas WT mice were largely insensitive to this stimulus intensity (Figure 4D). Only at high intensities (≥80 dB), ASR was also seen in most WT animals. Together, the sensorimotor phenotype of *Glra1*(D80A) mice resembles those of previously described GlyR mutants in mouse (*spasmodic*, *spastic*, or *oscillator)* and man (hyperekplexia) as well as the symptoms produced upon subconvulsive strychnine poisoning (Schofield, 2002).

Analysis of Glycine-Mediated Currents in *Glra1*(D80A) Spinal Neurons

To examine the functional consequences of the D80A substitution, we recorded GlyR currents in cultured spinal neurons prepared from E13 WT and homozygous *Glra1*(D80A) mice after 21 days of in vitro differentiation, i.e., a time period corresponding to the end of the second postnatal week. The analysis of glycine dose-response curves in these cultures revealed indistinguishable glycine potencies in cells from WT (EC_{50} = 27 ± 3.8 μM) and homozygous *Glra1*(D80A) mice (EC_{50} = 34 ± 5.3 μM; $n = 5$; $p > 0.05$; Figure 5A). Analysis of Zn^{2+} dose-response curves revealed a significant reduction in the potentiation of glycine currents by low concentrations of Zn^{2+} in cells from homozygous *Glra1*(D80A) mice as compared to WT neurons (53% ± 28% versus 117% ± 33% at 5 μM Zn^{2+}, respectively; $n = 7$; $p < 0.05$; Figure 5B). In contrast, Zn^{2+}-mediated inhibition at higher concentrations of the metal ion was not affected (Figure 5B).

In recombinant α1 GlyRs, the D80A substitution abolishes Zn^{2+} potentiation of glycine-mediated currents (Lynch et al., 1998). The residual Zn^{2+} potentiation seen in whole-cell currents recorded from homozygous *Glra1*(D80A) neurons may therefore reflect the expression of GlyR α subunits other than α1, which also are potentiated by low concentrations of Zn^{2+} (Laube et al., 1995). Immunostainings of the cultured neurons with an antibody specific for the perinatally expressed α2 subunit of the GlyR revealed that virtually all cells exhibiting α1 GlyR staining by mAb2b also showed α2

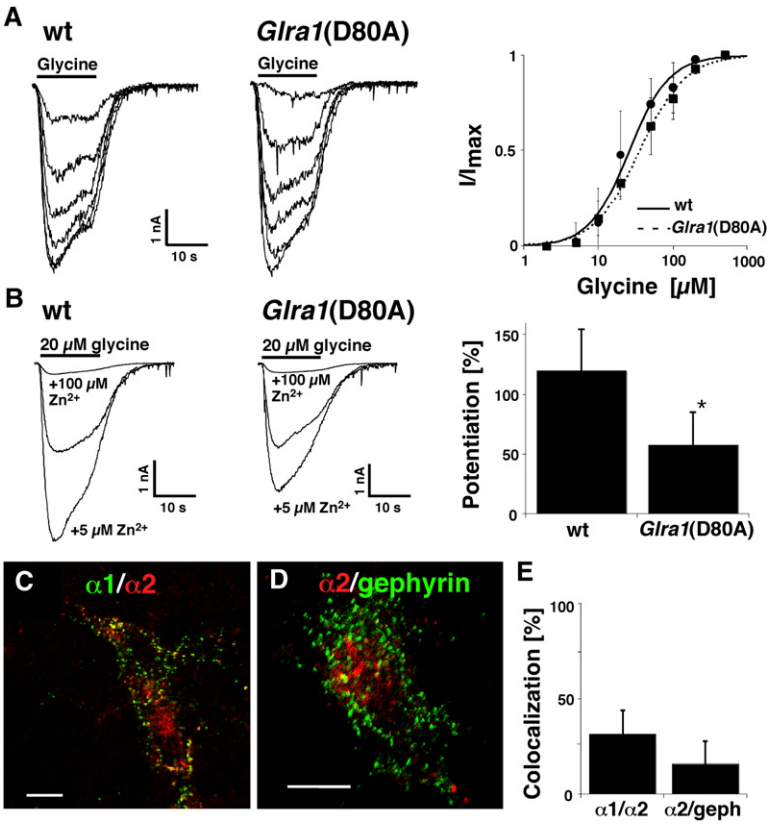

Figure 5. Electrophysiological Characterization of GlyR-Mediated Whole-Cell Currents Recorded from Cultured WT and Homozygous *Glra1*(D80A) Spinal Neurons after 21 Days In Vitro (DIV)

(A and B) Whole-cell patch-clamp analysis of glycine responses.

(A) Left: Responses of single cells to increasing concentrations of 10, 20, 50, 100, 200, and 500 μM glycine. Right: Pooled glycine dose-response curves for WT and homozygous *Glra1*(D80A) cells.

(B) Effect of Zn^{2+} on agonist-induced GlyR currents. Left: Traces represent potentiation and inhibition of responses to 20 μM glycine of WT and *Glra1*(D80A) neurons by 5 and 100 μM Zn^{2+}, respectively. Right: Average potentiation by 5 μM Zn^{2+} in WT and *Glra1*(D80A) cells (n = 5; $p < 0.05$).

(C) Immunostaining of individual neurons with GlyR α1 (green) and α2 (red) specific antibodies.

(D) Same, but immunostaining for the GlyR α2 subunit (red) and gephyrin (green). Colocalization is indicated in yellow. Scale bars, 10 μm.

(E) Quantification of GlyR α2 subunit colocalization in DIV21 cultured spinal neurons with the α1 subunit and gephyrin, respectively (n = 5, each).

Error bars indicate ± SEM.

GlyR immunoreactivity in double-staining experiments (Figure 5C). As demonstrated in Figure 5C, the α2 immunoreactivity was distributed over the entire cell and appeared to be less punctate as compared to the focal pattern found with antibodies against the α1 subunit or the postsynaptic GlyR clustering protein gephyrin (Figure 5D). Quantification of the immunoreactive structures revealed that only 28% ± 14% and 17% ± 13% (n = 5) of the α2 puncta colocalized with α1 and gephyrin, respectively (Figure 5E). Thus, most α2 GlyRs are not synaptically localized but represent extrasynaptic receptors. Consequently, the residual Zn^{2+} potentiation seen in homozygous *Glra1*(D80A) neurons mainly results from the modulation of nonsynaptic GlyRs.

Loss of Zn^{2+}-Mediated Potentiation of Glycinergic mIPSCs in Homozygous *Glra1*(D80A) Spinal Neurons

To investigate the effect of the D80A substitution on GlyR-mediated synaptic currents, we first analyzed the pharmacological properties of recombinant hetero-oligomeric α1β GlyRs, which are thought to be synaptically localized (Laube et al., 2002). Electrophysiological analysis of glycine dose responses revealed indistinguishable glycine EC_{50} values at WT α1β (EC_{50} = 74 ± 18 μM) and $\alpha1^{(D80A)}\beta$ (EC_{50} = 68 ± 13 μM; n = 4, each; $p > 0.05$) coexpressing human embryonic kidney (HEK)293 cells (Figure 6A). To reveal how the mutation affects Zn^{2+} modulation of hetero-oligomeric α1β GlyRs, Zn^{2+} dose-response curves were analyzed in the presence of submaximal (50 μM) and saturating (500 μM) glycine concentrations. Figure 6B shows that potentiation of glycine currents by low concentrations of Zn^{2+} was lost in HEK cells expressing $\alpha1^{(D80A)}\beta$ hetero-oligomers. Thus, the $\alpha1^{(D80A)}$ substitution suppresses Zn^{2+} potentiation in both homo- and hetero-oligomeric GlyRs. In contrast, at saturating glycine concentrations, where Zn^{2+} exerts only an inhibitory effect on glycine currents (Laube et al., 1995), no difference in the IC_{50} values of Zn^{2+} was found between WT α1β- and $\alpha1^{(D80A)}\beta$-expressing HEK cells (208 ± 41 μM and 167 ± 34 μM, respectively; n = 5; $p > 0.05$). This confirmed that the $\alpha1^{(D80A)}$ mutant selectively suppresses Zn^{2+}-mediated potentiation rather than inhibition of the heteromeric receptor. To exclude that the bath solution might be contaminated by low concentrations of Zn^{2+}, we added the chelator tricine (10 mM). This had no significant effect on both glycine currents (Figure 6B) and Zn^{2+} dose-response curves when recorded in defined Zn^{2+} buffers (data not shown; see Paoletti et al. [1997]). Similar results were obtained with 1 mM Ca^{2+}-EDTA, another effective Zn^{2+} chelator (data not shown). Thus, Zn^{2+} contamination was not relevant under our recording conditions.

We next examined the effect of the D80A substitution on synaptic currents by analyzing glycinergic mIPSCs in spinal cord cultures prepared from E13 WT and homozygous *Glra1*(D80A) mice after 21 days of in vitro differentiation (Figure 6C). Neurons from WT and homozygous *Glra1*(D80A) animals showed mIPSCs with variable, but similar frequencies (WT, 9.4 ± 5.2 Hz versus *Glra1*(D80A), 5.2 ± 4.2 Hz; n = 6; $p > 0.05$) and mean amplitudes (WT, 44 ± 14.7 pA versus *Glra1*(D80A), 49 ± 21.4 pA; n = 6; $p > 0.05$). Application of 500 nM strychnine abolished mIPSCs in both WT and homozygous *Glra1*(D80A)

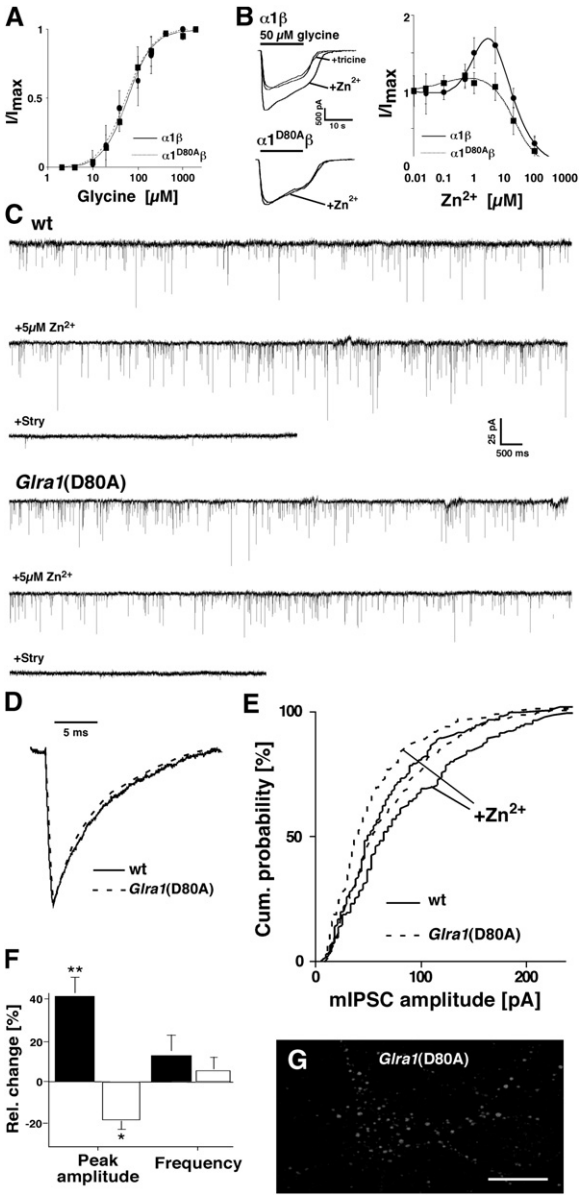

Figure 6. Electrophysiological Characterization of Synaptic $\alpha1^{D80A}$ GlyRs

(A and B) Whole-cell patch-clamp analysis of glycine responses elicited in HEK cells expressing $\alpha1\beta$ and $\alpha1^{D80A}\beta$ hetero-oligomeric GlyRs.

(A) Glycine dose-response curves for $\alpha1\beta$ and $\alpha1^{D80A}\beta$ cells.

(B) Current traces elicited by 50 μM glycine in the absence and presence of 5 μM Zn^{2+} (left) and respective Zn^{2+} dose-response curves (right) (n = 5, each). Note that addition of tricine (10 mM) had no effect on the glycine current.

(C–E) Glycinergic mIPSCs recorded from cultured spinal neurons of WT and homozygous *Glra1*(D80A) mice at DIV21.

(C) Consecutive traces showing mIPSCs prior to (upper trace) and during (middle trace) the application of 5 μM Zn^{2+} and in the presence (lower trace) of 500 nM strychnine (+Stry).

(D) Superimposed averaged glycinergic mIPSCs (n = 50) recorded from WT and homozygous *Glra1*(D80A) neurons. Note similar decay kinetics in both genotypes.

(E) Cumulative probability plot of mIPSCs amplitudes recorded prior to and during the application of 5 μM Zn^{2+} ($+Zn^{2+}$) from WT (solid lines) and homozygous *Glra1*(D80A) (dotted lines) neurons.

(F) Summary graph showing the relative changes in mIPSC mean amplitudes and frequencies found in WT and homozygous *Glra1*(D80A) neurons. Mean changes are expressed as percentages of control values obtained for mIPSCs recorded in the absence of Zn^{2+} for both WT (black bars) and homozygous *Glra1*(D80A) (white bars) neurons (n = 6; $p < 0.01$).

(G) Immunohistochemical localization of α1 subunit containing GlyR clusters in homozygous *Glra1*(D80A) spinal neurons at DIV21. Scale bar, 10 μm.

Error bars indicate ± SEM.

cultures, thereby confirming the glycinergic nature of the events recorded (Figure 6C). In addition, upon superposition of 50 mIPSC events, no differences were found in mIPSC decay kinetics between WT ($\tau = 11.2 \pm 1.8$ ms) and homozygous *Glra1*(D80A) ($\tau = 13.4 \pm 2.1$ ms; n = 5 each; $p > 0.05$) neurons, indicating that the D80A substitution does not alter the kinetic properties of basic glycinergic transmission (Figure 6D). We then added 5 μM Zn^{2+}, a concentration known to increase glycinergic mIPSC amplitude and frequency (Suwa et al., 2001; Laube, 2002) without potentiating currents of $\alpha1^{(D80A)}\beta$ hetero-oligomers (Figure 6B). Notably, in the presence of this low Zn^{2+} concentration mIPSC amplitudes were significantly inhibited in homozygous *Glra1*(D80A) neurons (−19% ± 6%; n = 6; $p < 0.05$; paired Student's t test), whereas in WT cells a mean increase of 41% ± 9% (n = 6; $p < 0.01$; paired Student's t test) was observed (Figure 6F). For example, the mean peak amplitudes of the representative mIPSCs shown in Figure 6C were 38 ± 14.3 pA (WT) and 41 ± 16.6 pA (*Glra1*(D80A)) in the absence of Zn^{2+}. After addition of 5 μM Zn^{2+}, the mean amplitudes of the mIPSCs shown in Figure 6C increased to 57 ± 23.4 pA for WT cells but decreased to 31 ± 12.1 pA in *Glra1*(D80A) neurons. In WT cultures, a decrease in mIPSC amplitude was only seen at higher Zn^{2+} concentrations (>20 μM) (see Laube [2002]). Cumulative probability histograms of the mIPSC amplitudes confirmed the observed reduction of the mean amplitude in homozygous *Glra1*(D80A) cells by a respective Zn^{2+}-induced shift toward the left, whereas WT cultures displayed an opposite effect upon Zn^{2+} addition (Figure 6E). In contrast, mIPSC frequencies were not differentially affected (Figure 6F). To confirm that under our culture conditions the α1 subunit was properly expressed and targeted to postsynaptic sites, the localization of GlyR α1(D80A) was examined by immunocytochemistry after 3 weeks in vitro. In both WT (data not shown) and homozygous *Glra1*(D80A) cells (Figure 6G), a typical membraneous punctate staining was produced by the α1 specific mAb2b antibody, as revealed upon confocal sectioning. Since these GlyR punctae are known to represent synaptically localized α1 containing GlyRs, this confirms proper expression and synaptic targeting of the mutant subunit in our cultures. These results are consistent with the D80A mutation affecting glycinergic inhibition by selectively eliminating Zn^{2+} potentiation of synaptically localized $\alpha1\beta$ GlyRs.

Altered Zn^{2+}-Dependence of Glycinergic IPSCs in Homozygous *Glra1*(D80A) Hypoglossal Motoneurons

To examine the effects of Zn^{2+} on glycinergic neurotransmission in situ, spontaneous IPSCs were recorded in hypoglossal motoneurons of acute brainstem slices

from P8 WT and homozygous *Glra1*(D80A) mice. At this age, α1 subunit containing GlyRs represent already >60% of the total GlyR protein in rodent spinal cord (Becker et al., 1992). Hypoglossal motoneurons from WT animals generated glycinergic IPSCs with a mean amplitude of 67.0 ± 27.0 pA and a decay time of τ = 13.5 ± 3.8 ms (n = 6; Figures 7A and 7B). In homozygous *Glra1*(D80A) neurons, mean IPSC amplitudes and decay kinetics were similar (67.3 ± 21.5 pA and τ = 12.3 ± 4.2 ms, respectively; n = 8; p > 0.05; Figures 7A and 7B). In addition, mean IPSC frequencies in WT and homozygous *Glra1*(D80A) cells were not statistically different (WT, 11.1 ± 5.1 Hz versus *Glra1*(D80A), 13.9 ± 3.4 Hz; n = 6; p > 0.05). Upon addition of 5 μM Zn^{2+}, a concentration which efficiently potentiates both recombinant $\alpha1\beta$ GlyRs and mIPSCs in dissociated spinal cultures, IPSCs were not potentiated, consistent with endogenous free Zn^{2+} being present in slice preparations at concentrations sufficient to preclude potentiation by the exogenously applied metal ion (Lu et al., 2000; Suwa et al., 2001). We therefore complexed endogenous Zn^{2+} by tricine (10 mM). This reduced the mean amplitude of IPSCs in WT slices by 44.1% ± 18.5% (from 67.0 ± 27.0 pA to 38.4 ± 24.2 pA; n = 6; p < 0.01; paired Student's t test; Figures 7A and 7C), while no significant effect on IPSC frequency was seen (11.1 ± 5.1 Hz versus 9.5 ± 5.2 Hz; n = 6; p > 0.05). Readjustment to a calculated free Zn^{2+} concentration of ca. 5 μM by adding 500 μM Zn^{2+} to the tricine buffer (Paoletti et al., 1997) resulted in a significant rescue of glycinergic IPSC mean amplitude (Figure 7A, increase by 35.4% ± 12.9%; n = 8; p < 0.05; paired Student's t test). This indicates that endogenous Zn^{2+} indeed contributes to the regulation of glycinergic IPSC amplitudes in our WT slice preparations. In contrast, slices made from homozygous *Glra1*(D80A) mice showed no significant effect of tricine on IPSC amplitude, with the mean amplitude being reduced by only 14.0% ± 8.6% (from 67.3 ± 21.5 pA to 57.7 ± 17.5 pA; n = 8; p > 0.05; paired Student's t test); again, no effect on IPSC frequencies was detected (13.9 ± 3.4 Hz versus 11.2 ± 3.8 Hz; n = 8; p > 0.05). Although mean IPSC amplitudes did not differ significantly between WT and homozygous *Glra1*(D80A) cells after the tricine treatment (38.4 ± 24.2 pA versus 57.7 ± 17.5 pA; n = 8; p = 0.054), the differential effects of tricine on IPSC mean amplitudes in WT and *Glra1*(D80A) preparations were highly significant (decrease in WT, 44.1% ± 18.4% versus *Glra1*, 12.8% ± 7.3%; n = 8; p < 0.001; Figure 7C). Moreover, the coefficient of variation calculated for the mean amplitude values was reduced upon tricine addition in the case of WT but not homozygous *Glra1*(D80A) slices (from 1.0 ± 0.37 to 0.7 ± 0.2 for WT; n = 8; p < 0.05, paired Student's t test, and from 0.78 ± 0.20 to 0.78 ± 0.27 for *Glra1*(D80A), respectively; p > 0.05, paired Student's t test). Thus, endogenous Zn^{2+} accounts for the higher variability of glycinergic IPSC amplitudes seen in WT as compared to homozygous *Glra1*(D80A) neurons.

To investigate whether tonic glycinergic inhibition mediated by extrasynaptic GlyRs may also be affected by Zn^{2+} chelation, we analyzed the holding currents (I_{hold}) of WT and *Glra1*(D80A) neurons before and after adding 10 mM tricine. Mean holding currents in WT and homozygous *Glra1*(D80A) cells were neither before (WT, −363 ± 191 pA versus. *Glra1*(D80A), −394 ± 139 pA) nor after the addition of tricine statistically different (WT, −425 ± 199 pA versus *Glra1*(D80A), −594 ± 157 pA; n = 8; p > 0.05, ANOVA). Apparently, ambient glycine concentrations do not contribute to tonic inhibition of hypoglossal motoneurons. Consistent with this interpretation, 1 μM strychnine did not alter I_{hold} values in both WT and *Glra1*(D80A) cells (WT, −201 ± 115 pA versus *Glra1*(D80A), −216 ± 117 pA; n = 8; p > 0.05, paired Student's t test). We conclude that tricine affects IPSCs primarily due to a loss of synaptic rather than extrasynaptic GlyR potentiation.

We also recorded sIPSCs from hypoglossal motoneurons of WT and homozygous *Glra1*(D80A) mice at P14–P16, i.e., at a stage at which the phenotype of the *Glra1*(D80A) mouse is fully manifest. Hypoglossal motoneurons from WT animals generated glycinergic IPSCs with a mean amplitude of 99.4 ± 8.0 pA and a decay time of τ = 6.97 ± 0.26 ms (n = 17, Figures 7D and 7E). In homozygous *Glra1*(D80A) neurons, mean IPSC amplitudes and decay times were significantly reduced (58.3 ± 7.7 pA and 2.99 ± 0.27 ms, respectively; n = 7; p < 0.01; Figure 7F). Thus, differences in IPSC characteristics apparently become detectable when the transition from α2- to α1-containing receptors is complete (Becker et al., 1992). Together, these data show that glycinergic IPSCs are altered in hypoglossal motoneurons of *Glra1*(D80A) mice due to a loss of Zn^{2+} potentiation.

Discussion

In this study, we report the first in vivo evidence for Zn^{2+} modulation of a ligand-gated ion channel in the mammalian CNS. By introducing a point mutation into the murine *Glra1* gene, we generated mice which display a severe hyperekplexia phenotype characterized by the development of inducible tremor, a delayed righting reflex, an abnormal gait, an increase in the b-wave amplitude of the ERG, and an enhanced ASR. These symptoms are hallmarks of impaired glycinergic neurotransmission (Schofield, 2002). As demonstrated by electrophysiological recordings in spinal cultures and brainstem slices, the *Glra1*(D80A) mutation caused a significant reduction in the Zn^{2+}-mediated potentiation of glycinergic IPSC amplitudes without altering basic GlyR function. Our results establish an essential role for Zn^{2+} in CNS inhibition and indicate that Zn^{2+} binding to synaptic GlyRs is crucial for proper sensorimotor coordination and function.

In murine spinal cord, the subunit composition of GlyRs changes during postnatal development (Becker et al., 1988). During the first and second postnatal week, the neonatal α2 subunit is replaced by adult α1 subunit containing receptors. At P8, $\geq$60% of the total GlyRs in WT spinal cord contain α1, and at P14 >90% (Becker et al., 1992). This GlyR isoform switch is the cause for the late onset of neuromotor symptoms at the end of the second postnatal week in the mutant mice *spasmodic* and *oscillator* which carry mutations in *Glra1* (Schofield, 2002). The appearance of the sensorimotor phenotype in *Glra1*(D80A) mice at around P12 thus coincides with the loss of GlyR α2 isoform expression and the onset of hyperekplexia symptoms in the natural *Glra1* mouse mutants. This suggests that the

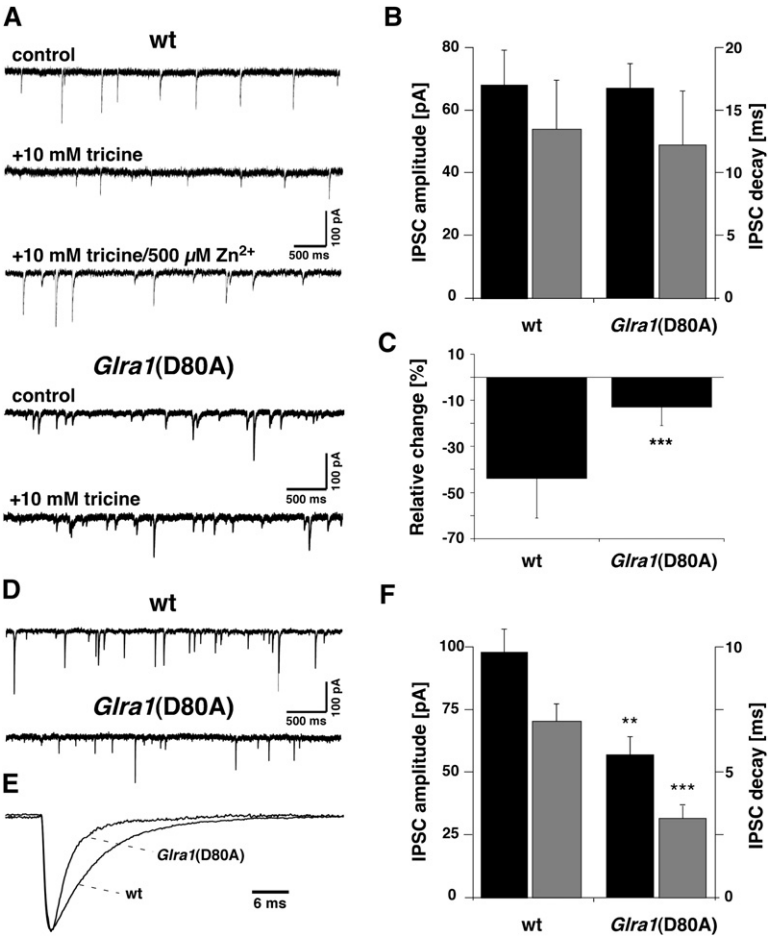

Figure 7. Spontaneous IPSCs Recorded from Hypoglossal Motoneurons In Situ

(A)–(C) P8; (D)–(F) P14.

(A) Typical spontaneous synaptic activity of hypoglossal motoneurons from P8 WT and homozygous *Glra1*(D80A) mice under control conditions, after application of tricine (10 mM) and after readjustment to a calculated free Zn^{2+} concentration of ca. 5 μM by adding 500 μM Zn^{2+} to the tricine buffer. Note the recovery of IPSC amplitude after readding Zn^{2+} to the WT slice.

(B) Mean amplitudes (black bars) and decay constants (gray bars) of spontaneous IPSCs recorded from P8 WT and homozygous *Glra1* (D80A) slices.

(C) Relative changes in mean amplitude of IPSCs caused by the addition of 10 mM tricine to slices from P8 WT and homozygous *Glra1*(D80A) mice.

(D) Typical spontaneous synaptic activity in hypoglossal motoneurons from P14 WT and homozygous *Glra1*(D80A) mice recorded under control conditions.

(E) Superimposed averaged glycinergic IPSCs (n = 50) recorded from P14 WT and in homozygous *Glra1*(D80A) neurons. Note different decay kinetics in both genotypes.

(F) Mean amplitudes (black bars) and decay constants (gray bars) of spontaneous IPSCs recorded from P14 WT and homozygous *Glra1*(D80A) slices.

Error bars indicate ± SEM.

developmental pattern of α1 subunit expression is unchanged in homozygous *Glra1*(D80A) mice.

Different lines of evidence indicate that the phenotype of homozygous *Glra1*(D80A) mice can be confidently attributed to a selective loss of synaptic Zn^{2+} potentiation. First, in heterologous expression experiments substitution of aspartate 80 by either glycine or alanine has been shown to selectively suppress Zn^{2+} potentiation of α1 GlyRs without altering the glycine dose-response relationship, open probability and single-channel conductance (Lynch et al., 1998; Laube et al., 2000). Similarly, here no changes in basic GlyR physiology could be detected with recombinant $\alpha1^{D80A}\beta$ GlyRs and homozygous *Glra1*(D80A) neurons. Second, GlyR expression and synaptic localization as monitored by Western analysis, [^{3}H]strychnine binding, and immunocytochemistry were not significantly altered in the homozygous mutant mice. Third, glycinergic IPSC amplitudes, decay kinetics, and frequencies were similar in cultured spinal neurons and P8 brainstemhypoglossal motoneurons prepared from WT and homozygous *Glra1*(D80A) animals. Only when recording glycinergic IPSCs from hypoglossal motoneurons at P14, i.e., a time point where the α2 to α1 subunit switch is complete and the hyperekplexia phenotype manifest, significantly reduced amplitudes and shorter decay times were found in *Glra1*(D80A) cells. This is consistent with ambient Zn^{2+} increasing the IPSC amplitudes and decay time of WT α1 but not *Glra1*(D80A) GlyRs (Suwa et al., 2001; Laube, 2002). Concurrently, chelation of Zn^{2+} by tricine disclosed comparable differences in glycinergic IPSCs between P8 WT and *Glra1*(D80A) hypoglossal neurons, confirming that the majority of GlyRs present at this stage contains the α1 subunit. Notably, the I_{hold} of the hypoglossal neurons was neither affected by strychnine nor tricine, indicating that the hyperekplexia phenotype of homozygous *Glra1*(D80A) mice is not due to altered tonic inhibition mediated by extracellular GlyRs. In contrast to our findings with homozygous *Glra1*(D80A) mice, the decrease in glycinergic IPSC amplitudes observed in *spasmodic* animals is caused by a reduced glycine affinity resulting from the A52S mutation in *Glra1* (Graham et al., 2006). In conclusion, the phenotype of *Glra1*(D80A) mice is due to impaired Zn^{2+} potentiation rather than a reduction or malfunctioning of the synaptically localized mutant GlyRs.

Earlier reports showing that histochemically detectable Zn^{2+} is highly enriched within glutamatergic mossy fiber terminals of the hippocampus had led to the proposal that synaptic Zn^{2+} modulates primarily excitatory neurotransmission (Li et al., 2003). Indeed, low micromolar concentrations of exogenous Zn^{2+} potently inhibit NMDA receptor currents (Paoletti et al., 1997). More recent studies revealed an enrichment of Zn^{2+} also in inhibitory nerve terminals (Velázquez et al., 1999; Danscher et al., 2001; Wang et al., 2001, 2002;

Danscher and Stoltenberg, 2005). At central synapses, the Zn^{2+} transporter ZnT3 is thought to accumulate Zn^{2+} within synaptic vesicles (Cole et al., 1999). The question therefore arises why homozygous *Glra1*(D80A) mice develop hyperekplexia, whereas no behavioral impairments have been found in ZnT3-deficient mice (Cole et al., 1999). One possible explanation could be that Zn^{2+} transporters other than ZnT3 mediate synaptic vesicle loading at inhibitory synapses where the consequences of ZnT3 deficiency have not been studied. Alternatively, nonvesicular mechanisms may allow for Zn^{2+} loading of and release from synaptic structures. ZnT3 independent accumulation of Zn^{2+} has been demonstrated in hippocampal neurons (Lee et al., 2000) and in synaptic regions of the developing barrel cortex (Liguz-Lecznar et al., 2005). Apparently, the large repertoire of 10 Slc30s (ZnT) and 14 Slc39s (Zip) genes allows to functionally compensate for ZnT3 deficiency which likely accounts for the lack of hyperekplexia symptoms in the ZnT3 knockout mice.

The basal concentrations of free Zn^{2+} at inhibitory synapses are unknown. However, in our brainstem slices, tricine reduced IPSC amplitudes and the corresponding coefficient of variation, whereas application of 5 μM Zn^{2+} had no effect. This again indicates that at least low micromolar concentrations of endogenous Zn^{2+} must have been present in our preparation. Zn^{2+} has been shown to not only increase the amplitude of GlyR responses at nonsaturating agonist concentrations (Laube et al., 2000) but to also inhibit glycine uptake mediated by the glial glycine transporter GlyT1 (Laube, 2002). Hence, Zn^{2+} might act synergistically by both potentiating postsynaptic GlyR currents and reducing glycine reuptake from the synaptic cleft, thereby producing a higher occupancy of the synaptic receptors. In conclusion, our in vivo data support the view that nonsaturating amounts of glycine are released during physiological inhibitory transmission.

Recent data indicate an enrichment of Zn^{2+} also in terminals of dorsal spinal and retinal neurons (Velázquez et al., 1999; Danscher et al., 2001; Ugarte and Osborne, 2001), suggesting that Zn^{2+} participates in the processing of sensory signals. Here, we found that *Glra1*(D80A) mice display profound changes in ERG and ASR. Our ERG recordings from *Glra1*(D80A) mice indicate an impaired glycinergic suppression of cone-mediated transmission. Endogenous Zn^{2+} levels are high in the vertebrate retina, and Zn^{2+} has been shown to modulate light responses of color-opponent bipolar and amacrine cells (Luo et al., 2002). Since the GlyR α1 subunit has been shown to localize at synapses between AII amacrine and bipolar cells (Haverkamp et al., 2004), we conclude from these morphological and functional data that the loss of Zn^{2+} potentiation at the α1(D80A) subunit reduces inhibition in the retina. This is consistent with the enhancement of the b-wave amplitude and the oscillatory potentials found in our experiments. Likewise, the enhanced ASR seen in the *Glra1*(D80A) mice suggests disinhibition of sensory input processing. In conclusion, our data reveal an essential role of endogenous Zn^{2+} in shaping sensory transmission within visual and auditory circuits.

The data presented in our paper disclose a pivotal role of ambient synaptic Zn^{2+} for glycinergic neurotransmission in the context of normal animal behavior. Whether activity-dependent alterations in extracellular Zn^{2+} concentration contribute to different forms of plasticity seen at inhibitory synapses, will have to be clarified in future studies. Our results imply that manipulation of synaptic Zn^{2+} levels by systemic Zn^{2+} intake or Zn^{2+}-specific chelators should affect glycinergic inhibition. Our work thus highlights the complexity of potential therapeutic interventions based on Zn^{2+}-selective chelation and/or Zn^{2+} supply (Doraiswamy and Finefrock, 2004), which may both perturb Zn^{2+} homeostasis and result in an imbalance of excitatory and inhibitory circuits.

Experimental Procedures

Generation of *Glra1*(D80A) ES Cells

A genomic fragment encompassing *Glra1* exons 4 to 6 was isolated from a P1 phage library. A 1 kb BglII-HindIII fragment containing exon 4 was subcloned, and the substitution D80A and an additional silent diagnostic XbaI restriction site were introduced by site-directed mutagenesis. The mutant BglII-HindIII fragment was then used to generate a D80A 6.1 kb HindIII fragment which formed the long arm of homology. This fragment was blunt-end inserted into HindIII/XbaI-digested pEasyflox, 5′ of the loxP site flanking the neomycin resistance cassette, thereby disrupting the XbaI site of the vector (Figure 1A). A 735 bp HindIII/XbaI short arm of homology was blunt end inserted into the BamHI site flanking the 3′-loxP site of the vector, disrupting the XbaI site of the genomic fragment. After linearization with NotI at the 3′-end of the short arm, the targeting construct was transfected into E14 ES cells. Colonies resistant to G-418 (Life Technologies) and 1-(2′-deoxy-2′-fluoro-β-D-arabinofuranosyl)-5-iodouracil (FIAU) were selected and screened for homologous integration of the construct by PCR using primers P1 (TGCTG GGGGAAACTTCCTGACTAGG) and P2 (TGCTGAGTGTCCTTGGGA CCATCAC) (Figure 1A). Homologous recombination events were confirmed by Southern blot analysis. Removal of the loxP-flanked neomycin cassette was achieved by transfection with the Cre recombinase expression plasmid pgkCrebpA and verified by PCR using primers P3 (GCCTACAATGAATACCCTGCCGATAG) and P4 (GGACACTCTGAAAGCTGATCCATAACTTC), as well as by Southern blot analysis.

Generation of *Glra1*(D80A) Mice

Glra1(D80A) homozygous mutant mice were produced by injecting ES cells with one engineered *Glra1*(D80A) allele into C57BL/6 blastocysts, which resulted in germline-transmitting chimeras. With C57BL/6 females, these animals sired offspring heterozygous for the mutation. For the analysis of sensorimotor behavior, chimeras were backcrossed over five generations to C57BL/6 females, and heterozygous offspring were then interbred to yield all genotypes.

Southern Blot Analysis

Genomic DNA of ES cells or mouse tissue was digested with XbaI, or BclI and XbaI, separated by agarose gel electrophoresis, and transferred to Hybond N^+ membrane (Amersham). ^{32}P-labeled internal probes were generated by random primer labeling (Prime It II, Stratagene) of a 735 bp HindIII/XbaI fragment and hybridized to the membrane.

Miscellaneous Methods

Western blot analysis of crude membrane fractions prepared from mouse spinal cord with antibodies specific for GlyR α subunits (mAb4a, 1:1000), the GlyR α1 subunit (mAb2b, 1:100), and syntaxin (1:5000) and glycine-displaceable binding of [^{3}H]strychnine (DuPont NEN) were performed as described previously (Becker et al., 1988). Western blots were scanned, and digitalized images were analyzed for quantification using the software NIH-Image 1.63.

Behavioral Characterization of *Glra1*(D80A) Mice

The methods used for monitoring the neuromotor performance of *Glra1*(D80A) mice (hind feet clasping, tremor recordings, righting

response quantification) have been described previously (Becker et al., 2002). Footprint tracings were generated using P20–P30 mice from four different breeding pairs. Mouse footpads were painted with Tempera paint, and mice were placed onto a sheet of paper in a 50 cm long tube. The ASR was measured as described (Plappert and Pilz, 2001). The protocol was designed to determine strain sensitivity to startle stimuli of three intensities between 70 and 90 dBs presented randomly in 50 ms pulses, with an interval of 30 s. In this protocol each mouse experienced 10 trials at each noise level. ERGs were obtained as previously described (Seeliger et al., 2001). At the age of 3 months, mice were dark adapted overnight and anesthetized with ketamine (66.7 mg/kg) and xylazine (11.7 mg/kg). The pupils were dilated, and single-flash ERG recordings were obtained under scotopic (DA) and photopic (LA) conditions. Stimuli were presented with increasing intesities, reaching from 10^{-4} cd * s/M2 to 25 cd * s/m^2, divided into ten steps. Ten responses were averaged with an interstimulus interval (ISI) of 5 s (for 0.1, 1, 10, 30, 100, 300 mcd*s/m^2), 10 s (for 1 and 3 cd*s/m^2), or 20 s (for 10 and 25 cd*s/m^2). In all tests conducted, WT littermates served as controls for the respective homozygous mutant animals. All procedures were approved by the animal care committee and were in accordance with the German law on animal experimentation.

Spinal Cord Cultures and Immunochemistry

Spinal cord cultures were prepared from E13 mice and kept in culture for 3 weeks as described (Laube, 2002). Immunolabeling of spinal cord sections was performed as detailed previously (Kneussel et al., 1999), using primary antibodies to the postsynaptic GlyR clustering protein gephyrin (1:100) and the GlyR subunits α1 and α2 (1:100). MAb2b is specific for the GlyR α1 subunit; mAb4a recognizes all GlyR α subunits. A polyclonal goat antibody against the N-terminal 18 residues of the GlyR α2 subunit was purchased from Santa Cruz Biotechnology. Confocal microscopy was performed using a confocal laser-scanning microscope Leica TCS-SP equipped with the image software Leica-TCS-NT version 1.6.551. To obtain spinal cord sections, tissue was cut in blocks of 5 mm and immediately frozen. Cryostat sections (12 μM) were fixed for 2 min in 4% (w/v) paraformaldehyde and processed for immunofluorescence. Punctate immunofluorescence was analyzed from confocal images taken with a 63× objective. The number of puncta per 100 μm^2 was counted from three different sections. Between 400 and 600 individual puncta were analyzed for the α1 GlyR subunit in WT and *Glra1*(D80A) samples.

Electrophysiological Recording of Agonist-Evoked and mIPSCs

Whole-cell currents of transfected HEK293 (ATCC CRL 1573) were analyzed as described previously (Laube et al., 2000). Cultured cells were continuously superfused (0.5 ml per min) at room temperature with an extracellular bathing solution containing 137 mM NaCl, 5.4 mM KCl, 1.8 mM $CaCl_2$, 1.0 mM $MgCl_2$, 20 mM glucose, and 10 mM HEPES; adjusted to pH 7.2 with NaOH. Patch pipettes contained 120 mM CsCl, 20 mM tetraethylammonium chloride, 1 mM $CaCl_2$, 2 mM $MgCl_2$, 1 mM ATP, 11 mM EGTA, and 10 mM HEPES (pH 7.2). Agonist-induced currents and mIPSCs in cultured spinal neurons were recorded from neuronal somata in the whole-cell configuration of the patch-clamp technique (Laube, 2002).

Electrophysiological Recordings from Acutely Isolated Hypoglossal Slices

Three hundred micrometer slices (Vibroslicer, Leica VT 1000S, Leica Instruments) of the caudal medulla containing the hypoglossal nucleus from P8 or P14–P16 mice were prepared as described previously (Gomeza et al., 2003). Slices were stored for 1 hr at 37°C in a modified ACSF containing 118 mM NaCl, 3 mM KCl, 1 mM $CaCl_2$, 5 mM $MgCl_2$, 1 mM NaH_2PO_4, 25 mM $NaHCO_3$, and 10 mM D-glucose (pH 7.4). After a 1 hr preincubation, the slices were stored in ACSF until transfer to a recording chamber. Hypoglossal motoneurons were identified visually by their location, size, and shape. Whole-cell recordings were obtained at 21°C–24°C with a L/M-PCA patch clamp amplifier (E.S.F.). Patch electrodes were pulled from borosilicate glass capillaries (Biomedical Instruments) on a programmable pipette-puller (Zeitz Instruments) and had resistances ranging from 2 to 4 MΩ when filled with intracellular solution containing 110 mM CsCl, 30 mM TEA-Cl, 1 mM $CaCl_2$, 2 mM $MgCl_2$, 4 mM Na_2ATP, 10 mM HEPES, 10 mM EGTA (pH adjusted to 7.2 with KOH). 5-Lidocaine-*N*-ethyl bromide (QX-314, 5 mM) was added to the electrode solution to intracellularly block fast sodium currents. Currents were filtered at 3 kHz with a four-pole Bessel filter and digitized at 10 kHz using a PowerLab inteface and Chart 4.2 software (ADInstruments Pty. Ltd.). Spontaneous IPSC recordings were isolated by adding 20 μM 6-cyano-7-nitroquinoxaline-2,3-dione (CNQX), 100 μM DL-2-amino-5-phosphonopentanoate (AP5), and 20 μM bicuculline and analyzed using the MiniAnalysis program (Jaejin Software) as described (Gomeza et al., 2003). To test the effect of extracellular Zn^{2+} (used as $ZnCl_2$) on GlyRs in situ, tricine (10 mM) was added. For calculation of the time constants of IPSC decays, only IPSCs that were larger then the averaged amplitude of the recorded IPSC and clearly separated form each other were used. Spontaneous IPSC decay phases were fit by two exponentials, and the mean time constant, t_{decay}, was calculated from the respective time constants and their relative amplitudes (a_1,a_2)—$t_{decay} = t_1a_1 + t_2a_2$ using MiniAnalysis Program.

Statistical Analysis

Results represent means ± SEM. Differences were tested by Student's two-tailed t test using GraphPad Prism version 4.0 (GraphPad Software Inc.), if not indicated otherwise, and considered to be statistically significant at $p < 0.05$ (*), $p < 0.01$ (**), and $p < 0.001$ (***). Homozygous *Glra1*(D80A) mice were compared to WT littermates and age-matched C57B6 control mice.

Acknowledgments

This study was supported by Deutsche Forschungsgemeinschaft (La 1086/2-2, SFB 406, DFG-Forschungszentrum für Molekular-Physiologie des Gehirns), Bundesministerium für Bildung und Forschung (01KV0002), and Fonds der Chemischen Industrie. We thank Prof. H. Wässle for critically reading the manuscript, Drs. J. Gomeza and H. Weiher for advice on analyzing mutant mice, Dr. M. Kössl for providing the setup for acoustic stimulation, Dr. K. Rajewski for the gift of pEasyflox and pgkCrebpA, and Ina Bartnik and Elena Zurkowski for technical assistance.

Received: March 23, 2006
Revised: August 8, 2006
Accepted: September 18, 2006
Published: November 21, 2006

References

Assaf, S.Y., and Chung, S.H. (1984). Release of endogenous Zn^{2+} from brain tissue during activity. Nature *308*, 734–735.

Baranano, D.E., Ferris, C.D., and Snyder, S.H. (2001). Atypical neural messengers. Trends Neurosci. *24*, 99–106.

Becker, C.M., Hoch, W., and Betz, H. (1988). Glycine receptor heterogeneity in rat spinal cord during postnatal development. EMBO J. *7*, 3717–3726.

Becker, C.M., Schmieden, V., Tarroni, P., Strasser, U., and Betz, H. (1992). Isoform-selective deficit of glycine receptors in the mouse mutant spastic. Neuron *8*, 283–289.

Becker, L., von Wegerer, J., Schenkel, J., Zeilhofer, H.U., Swandulla, D., and Weiher, H. (2002). Disease-specific human glycine receptor α1 subunit causes hyperekplexia phenotype and impaired glycine- and $GABA_A$-receptor transmission in transgenic mice. J. Neurosci. *22*, 2505–2512.

Betz, H., and Laube, B. (2006). Glycine receptors: recent insights into their structural organization and functional diversity. J. Neurochem. *97*, 1600–1610.

Bloomenthal, A.B., Goldwater, E., Pritchett, D.B., and Harrison, N.L. (1994). Biphasic modulation of the strychnine-sensitive glycine receptor by zinc. Mol. Pharmacol. *46*, 1156–1159.

Chandra, T., Maier, W., König, H., Hirzel, K., Kögel, D., Schüler, T., Chandra, A., Demirhan, I., and Laube, B. (2005). Molecular interactions of the type 1 human immunodefiency virus tat protein with N-methyl-D-aspartate receptor subunits. Neuroscience *134*, 145–153.

Chen, C.J., and Liao, S.L. (2003). Neurotrophic and neurotoxic effects of zinc on neonatal cortical neurons. Neurochem. Int. *42*, 471–479.

Choi, D.W., and Koh, J.Y. (1998). Zinc and brain injury. Annu. Rev. Neurosci. *21*, 347–375.

Cole, T.B., Wenzel, H.J., Kafer, K.E., Schwartzkroin, P.A., and Palmiter, R.D. (1999). Elimination of zinc from synaptic vesicles in the intact mouse brain by disruption of the ZnT3 gene. Proc. Natl. Acad. Sci. USA *96*, 1716–1721.

Danscher, G., and Stoltenberg, M. (2005). Zinc-specific autometallographic *in vivo* selenium methods: tracing of zinc-enriched (ZEN) terminals, ZEN pathways, and pools of zinc ions in a multitude of other ZEN cells. J. Histochem. Cytochem. *53*, 141–153.

Danscher, G., Jo, S.M., Varea, E., Wang, Z., Cole, T.B., and Schröder, H.D. (2001). Inhibitory zinc-enriched terminals in mouse spinal cord. J. Neurosci. *105*, 941–947.

Doraiswamy, P.M., and Finefrock, A. (2004). Metals in our minds: therapeutic implications for neurodegenerative disorders. Lancet Neurol. *3*, 431–434.

Gomeza, J., Ohno, K., Hülsmann, S., Armsen, W., Eulenburg, V., Richter, D.W., Laube, B., and Betz, H. (2003). Deletion of the mouse glycine transporter 2 results in a hyperekplexia phenotype and postnatal lethality. Neuron *40*, 797–806.

Graham, B.A., Schofield, P.R., Sah, P., Margrie, T.W., and Callister, R.J. (2006). Distinct physiological mechanisms underlie altered glycinergic synaptic transmission in the murine mutants spastic, spasmodic, and oscillator. J. Neurosci. *26*, 4880–4890.

Harvey, R.J., Thomas, P., James, C.H., Wilderspin, A., and Smart, T.G. (1999). Identification of an inhibitory Zn^{2+} binding site on the human glycine receptor a1 subunit. J. Physiol. *520*, 53–64.

Haverkamp, S., Müller, U., Zeilhofer, H., Harvey, R., and Wässle, H. (2004). Diversity of glycine receptors in the mouse retina: localization of the a2 subunit. J. Comp. Neurol. *477*, 399–411.

Jo, S.M., Danscher, G., Schröder, H.D., Won, M.H., and Cole, T.B. (2000). Zinc-enriched (ZEN) terminals in mouse spinal cord: immunohistochemistry and autometallography. Brain Res. *870*, 163–169.

Kambe, T., Yamaguchi-Iwai, Y., Sasaki, R., and Nagao, M. (2004). Overview of mammalian zinc transporters. Cell. Mol. Life Sci. *61*, 49–68.

Kay, A.R. (2006). Imaging synaptic zinc: promises and perils. Trends Neurosci. *29*, 200–206.

Kneussel, M., Brandstätter, J.H., Laube, B., Stahl, S., Müller, U., and Betz, H. (1999). Loss of postsynaptic $GABA_A$ receptor clustering in gephyrin-deficient mice. J. Neurosci. *19*, 9289–9297.

Laube, B. (2002). Potentiation of inhibitory glycinergic neurotransmission by Zn^{2+}: a synergistic interplay between presynaptic P2X2 and postsynaptic glycine receptors. Eur. J. Neurosci. *16*, 1025–1036.

Laube, B., Kuhse, J., Rundström, N., Kirsch, J., Schmieden, V., and Betz, H. (1995). Modulation by zinc ions of native rat and recombinant human inhibitory glycine receptors. J. Physiol. *483*, 613–619.

Laube, B., Kuhse, J., and Betz, H. (2000). Kinetic and mutational analysis of Zn^{2+} modulation of recombinant human inhibitory glycine receptors. J. Physiol. *522*, 215–230.

Laube, B., Maksay, G., Schemm, R., and Betz, H. (2002). Modulation of glycine receptor function: a novel approach for therapeutic intervention at inhibitory synapses? Trends Pharmacol. Sci. *23*, 519–527.

Lee, J.Y., Cole, T.B., Palmiter, R.D., and Koh, J.Y. (2000). Accumulation of zinc in degenerating hippocampal neurons of ZnT3-null mice after seizures: evidence against synaptic vesicle origin. J. Neurosci. *20*, 1–5.

Li, Y., Hough, C.J., Suh, S.W., Sarvey, J.M., and Frederickson, C.J. (2001). Rapid translocation of Zn^{2+} from presynaptic terminals into postsynaptic hippocampal neurons after physiological stimulation. J. Neurophysiol. *86*, 2597–2604.

Li, Y.V., Hough, C.J., and Sarvey, J.M. (2003). Do we need zinc to think? Sci. STKE *182*, pe19.

Liguz-Lecznar, M., Nowicka, D., Czupryn, A., and Skangiel-Kramska, J. (2005). Dissociation of synaptic zinc level and zinc transporter 3 expression during postnatal development and after sensory deprivation in the barrel cortex of mice. Brain Res. Bull. *66*, 106–113.

Lu, Y.M., Taverna, F.A., Tu, R., Ackerley, C.A., Wang, Y.T., and Roder, J. (2000). Endogenous Zn^{2+} is required for the induction of long-term potentiation at rat hippocampal mossy fiber-CA3 synapses. Synapse *38*, 187–197.

Luo, D.G., Li, G.L., and Yang, X.L. (2002). Zn^{2+} modulates light responses of color-opponent bipolar and amacrine cells in the carp retina. Brain Res. Bull. *58*, 461–468.

Lynch, J.W. (2004). Molecular structure and function of the glycine receptor chloride channel. Physiol. Rev. *84*, 1051–1096.

Lynch, J.W., Jacques, P., Pierce, K.D., and Schofield, P.R. (1998). Zinc potentiation of the glycine receptor chloride channel is mediated by allosteric pathways. J. Neurochem. *71*, 2159–2168.

Miller, P.S., Da Silva, H.M., and Smart, T.G. (2005). Molecular basis for zinc potentiation at strychnine-sensitive glycine receptors. J. Biol. Chem. *280*, 37877–37884.

Paoletti, P., Ascher, P., and Neyton, J. (1997). High-affinity zinc inhibition of NMDA NR1-NR2A receptors. J. Neurosci. *17*, 5711–5725.

Plappert, C.F., and Pilz, P. (2001). The acoustic startle response as an effective model for elucidating the effect of genes on the neural mechanism of behavior in mice. Behav. Brain Res. *125*, 183–188.

Qian, J., and Noebels, J.L. (2005). Visualization of transmitter release with zinc fluorescence detection at the mouse hippocampal mossy fibre synapse. J. Physiol. *566*, 747–758.

Schofield, P.R. (2002). The role of glycine and glycine receptors in myoclonus and startle syndromes. Adv. Neurol. *89*, 263–274.

Seeliger, M.W., Grimm, C., Stahlberg, F., Friedburg, C., Jaissle, G., Zrenner, E., Guo, H., Remé, C., Humphries, P., Hofmann, F., et al. (2001). New views on RPE65 deficiency: the rod system is the source of vision in a mouse model of Leber congenital amaurosis. Nat. Genet. *29*, 70–74.

Smart, T.G., Hosie, A.M., and Miller, P.S. (2004). Zn^{2+} ions: modulators of excitatory and inhibitory synaptic activity. Neuroscientist *10*, 432–442.

Suwa, H., Saint-Amant, L., Triller, A., Drapeau, P., and Legendre, P. (2001). High affinity zinc potentiation of inhibitory postsynaptic glycinergic currents in the zebrafish hindbrain. J. Neurophysiol. *85*, 912–926.

Ugarte, M., and Osborne, N.N. (2001). Zinc in the retina. Prog. Neurobiol. *64*, 219–249.

Velázquez, R.A., Cai, Y., Shi, Q., and Larson, A.A. (1999). The distribution of zinc selenite and expression of metallothionein-III mRNA in the spinal cord and dorsal root ganglia of the rat suggest a role for zinc in sensory transmission. J. Neurosci. *19*, 2288–2300.

Vogt, K., Mellor, J., Tong, G., and Nicoll, R. (2000). The actions of synaptically released zinc at hippocampal mossy fiber synapses. Neuron *26*, 187–196.

Wang, Z., Li, J.Y., Dahlstrom, A., and Danscher, G. (2001). Zinc-enriched GABAergic terminals in mouse spinal cord. Brain Res. *921*, 165–172.

Wang, Z., Danscher, G., Kim, Y.K., Dahlstrom, A., and Mook Jo, S. (2002). Inhibitory zinc-enriched terminals in the mouse cerebellum: double-immunohistochemistry for zinc transporter 3 and glutamate decarboxylase. Neurosci. Lett. *321*, 37–40.